

## *Supplementary Information*

# **Photo-Induced Cation Exchange Reaction of Germanium Chalcogenide Nanocrystals Synthesized Using Gas-Phase Laser Photolysis Reaction**

Yoon Myung, Hyung Soon Im, Chang Hyun Kim, Chan Su Jung, Yong Jae Cho, Dong Myung Jang, Han Sung Kim, Seung Hyuk Back, and Jeunghee Park\*

## **Experimental**

Laser photolysis of tetramethyl germanium (TMG, 98%, Sigma-Aldrich), H<sub>2</sub>S, dimethyl selenium (DMS, 98%, Sigma-Aldrich) mixture was performed using an 1064 nm Nd-YAG pulsed laser (Coherent SL-10) operating with a repetition rate of 10 Hz and a pulse width of 10 ns. Gas sources were degassed by several freeze (77 K)-pump-thaw cycles, then used without further purification. The precursor vapors (5-50 Torr) were introduced to a 1L volume pyrex glass reactor, equipped with a gas valve connecting to a standard vacuum line and a 2-inch diameter quartz optical window. The laser beam was focused into the closed reactor with a 10-cm focal length lens through the window. The experiment was carried using the laser intensity 0.1~0.2 J/pulse. After 1~3 h laser irradiation, the gas products were vented and the free-standing NC powders were collected by dispersing them in ethanol, followed by evaporation and vacuum drying at room temperature. For thermal annealing of GeX NC to produce the crystalline phase, the NC powders were placed in a quartz tube at 250~450 °C under Ar flow (50-100 sccm), for 30 min~1 h.

For the cation-exchange reaction, we prepared 0.01 M GeX and 0.1 M Zn(NO<sub>3</sub>)<sub>2</sub> (or Cd(NO<sub>3</sub>)<sub>2</sub>, Pb(NO<sub>3</sub>)<sub>2</sub>) aqueous solutions. In the case of AgNO<sub>3</sub>, 0.02 M and 0.05 M solution were used. Light irradiation of a 450 W Xe lamp (Oriel) can accelerate to exchange reaction. The reaction time was varied from a few minutes to 1 h, depending on the cation. After the reaction, the NC products were precipitated by centrifuging the reaction mixture. The NC precipitates were rinsed with methanol for further characterization of their structure and composition.

The products were analyzed by field-emission transmission electron microscopy (TEM, Jeol JEM 2100F and FEI TECNAI G<sup>2</sup> 200 kV), high-voltage TEM (HVEM, Jeol JEM ARM 1300S, 1.25 MV), and energy-dispersive X-ray fluorescence spectroscopy (EDX). High-resolution X-ray diffraction (XRD) patterns were obtained using the 9B and 3D beam lines of the Pohang Light Source (PLS) with monochromatic radiation ( $\lambda=1.54595 \text{ \AA}$ ). X-ray photoelectron spectroscopy (XPS) was performed using the 8A1 beam line of the PLS and a laboratory-based spectrometer (ESCALAB 250, VG Scientifics) using a photon energy of 1486.6 eV (Al K $\alpha$ ).

**Figure S1.** (a) XRD pattern of NC as the pressure ratio ( $y$ ) of the reactants,  $y = p_{\text{H}_2\text{S}}/p_{\text{TMG}} = [\text{H}_2\text{S}]/[\text{TMG}]$  or  $p_{\text{DMS}}/p_{\text{TMG}} = [\text{DMS}]/[\text{TMG}]$ , increases. The peaks of Ge NC are matched to that of the reference peaks of cubic phase Ge (JCPDS No. 04-0545,  $a = 5.6576 \text{ \AA}$ ). (b) The composition of NC ( $=[\text{S}]/[\text{Ge}]$  or  $[\text{Se}]/[\text{Ge}]$ ) versus that of gas-phase reactants. The composition of NC is identified by EDX and XPS. (c) The HRTEM and FFT images of crystalline Ge NC reveals that the (111) fringes are separated by a distance of about 3.3  $\text{\AA}$ , corresponding to that of cubic phase Ge.

The  $[S]/[Ge]$  ratio of NC is linearly increased to 1.8, as  $y$  is increased to 2, but did not increase thereafter. In contrast, the  $[Se]/[Ge]$  ratio is steadily increased to 5, as  $y$  is increased to 5. As described in the text,  $H_2S$  decomposed by the reaction with the Ge atoms;  $nGe^* + nH_2S \rightarrow GeS^* + nH_2$ . We checked no S formation from the  $H_2S$  alone. It was observed that the higher  $[H_2S]/[TMG]$  ratio results in the less yield. These results indicate that as the excess  $H_2S$  quench the growth reaction of GeS NC, the yield decreases and the products would have a deficient S composition. In the case of Se, amorphous Se element is produced from the DMS alone. The steady increase of the  $[Se]/[Ge]$  ratio is due to the separated formation of amorphous Se element from the excess DMS. The XPS data also show the production of Se element (see Figure S2). Therefore the high  $[DMS]/[TMG]$  ratio increases the yield of Se, which increase the  $[Se]/[Ge]$  ratio of products.

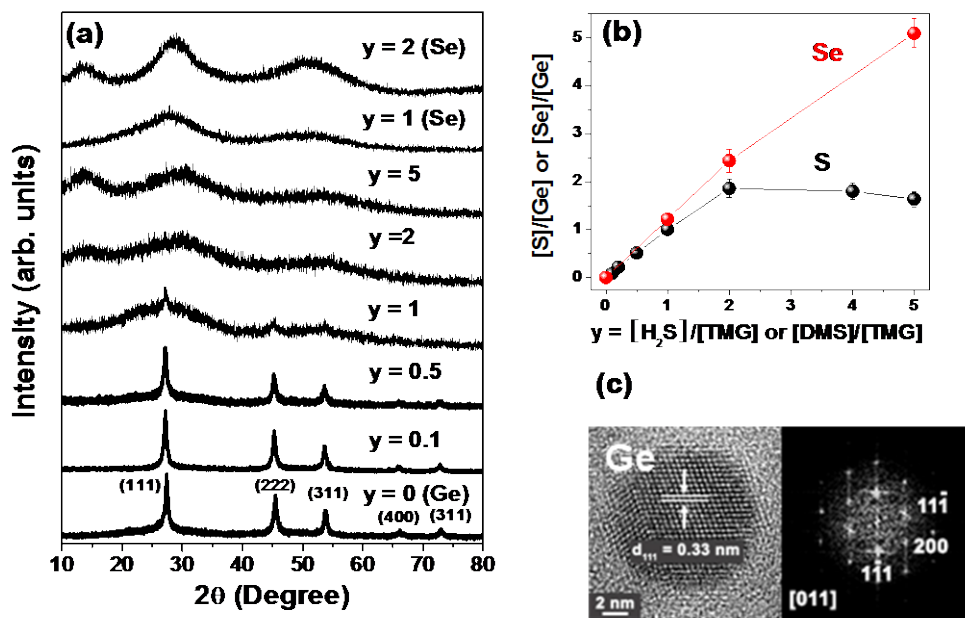


**Figure S2.** (a) Survey-scan XPS, and fine-scanned (b) Ge 3d, (c) S 2p, and (d) Se 3d peaks of  $\text{GeS}_x$  ( $x = 1$  and 2), and  $\text{GeSe}_x$  ( $x = 1$  and 2). The binding energy of Ge 3d shows a blue shift as the composition of S or Se increases, indicating a larger oxidation number of the Ge cation. In the case of GeSe NC, the binding energy is higher than that of GeS NC, probably due to the higher electronegativity of Se; Pauling's value  $\chi(\text{Ge}) = 2.0$ ,  $\chi(\text{S}) = 2.4$ ,  $\chi(\text{Se}) = 2.5$ .  $\text{GeSe}_2$  NC exhibit a slight red shift from that of GeSe, which is probably related with the presence of Se element phase (as discussed below). The peak positions of GeSe and  $\text{GeSe}_2$  NC are consistent with the reference values of the bulk [Handbook of X-ray Photoelectron Spectroscopy, John F. Moulder *et al.* 1995, Physical Electronics Inc.]. Therefore, the amorphous GeX NC contains the Ge cation whose oxidation number is close to that of the crystalline phase.

The binding energy of S 2p of GeS and  $\text{GeS}_2$  NC shows a red shift (2.4 eV) from that of the bulk S (164 eV). This shift is ascribed to the electron density increase upon coordination with the Ge cation, which in turn produces the S anion. The Se 3d peak of GeSe and  $\text{GeSe}_2$  NC consisted of two resolved bands (by using a Voigt function), corresponding to two binding states; one is the Se element (55.6 eV) and another is the anion form which is red shifted by ~2 eV. As the Se composition increases, the fraction of the Se element increases. In fact, the ratio of  $[\text{Se}]/[\text{Ge}]$  is 1.2 and 2.4, respectively, for GeSe and  $\text{GeSe}_2$  (see EDX data of Figure S2). After the 1:1 or 1:2 binding, excess Se element exists probably as the amorphous form.

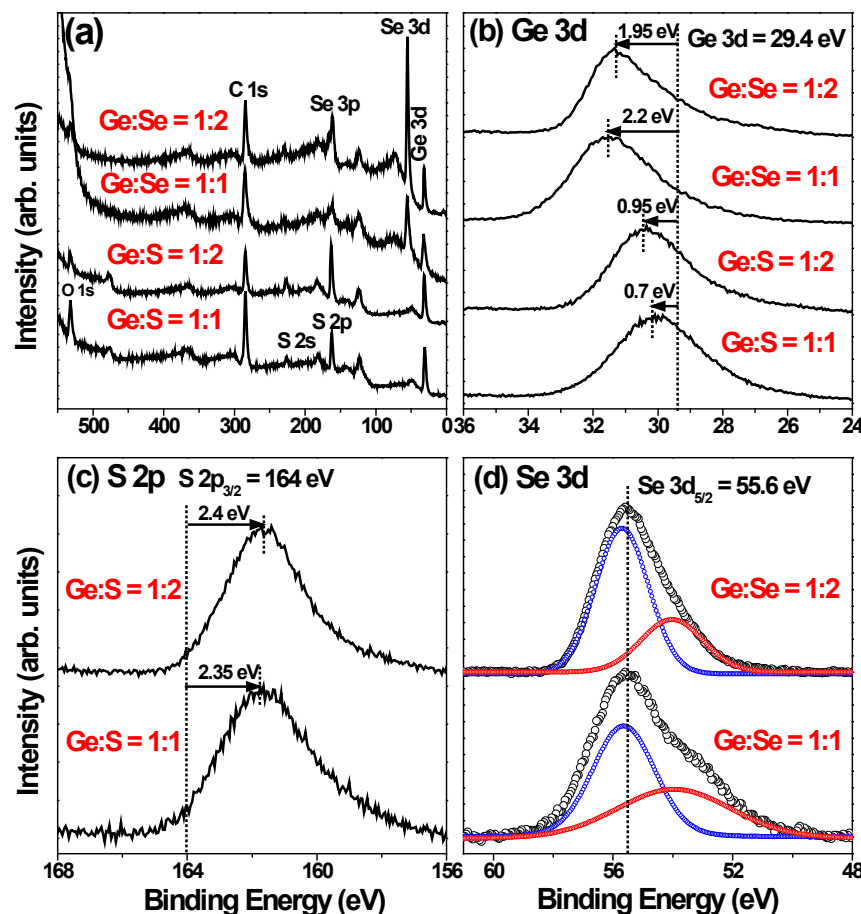


**Figure S3.** XRD pattern of GeS, GeS<sub>2</sub>, GeSe, and GeSe<sub>2</sub> NC, synthesized *via* thermal annealing of amorphous NC. The thermal annealing of amorphous GeS NC at 250 °C (30 min) under Ar ambient produces the orthorhombic phase GeS, whose peaks are exactly matched to those of the bulk orthorhombic GeS (JCPDS No. 85-1114;  $a = 4.290 \text{ \AA}$ ,  $b = 10.42 \text{ \AA}$ ,  $c = 3.640 \text{ \AA}$ ). The thermal annealing of amorphous GeS<sub>2</sub> NC at 350 °C yields the crystalline GeS<sub>2</sub> NC, whose XRD peaks are exactly matched to those of the bulk monoclinic GeS<sub>2</sub> (JCPDS No. 30-0597;  $a = 6.875 \text{ \AA}$ ,  $b = 22.55 \text{ \AA}$ ,  $c = 6.809 \text{ \AA}$ ,  $\beta=120.45^\circ$ ). The thermal annealing of amorphous GeSe and GeSe<sub>2</sub> NC at 350 and 450 °C (1 h) produces orthorhombic GeSe and monoclinic GeSe<sub>2</sub>, respectively. The peaks

are assigned by the reference of the bulk; GeSe (JCPDS No. 74-0372;  $a = 4.400 \text{ \AA}$ ,  $b = 3.850 \text{ \AA}$ ,  $c = 10.820 \text{ \AA}$ ) and  $\text{GeSe}_2$  (JCPDS No. 71-0117;  $a = 7.061 \text{ \AA}$ ,  $b = 16.79 \text{ \AA}$ ,  $c = 11.831 \text{ \AA}$ ,  $\beta=90.650^\circ$ ), respectively.

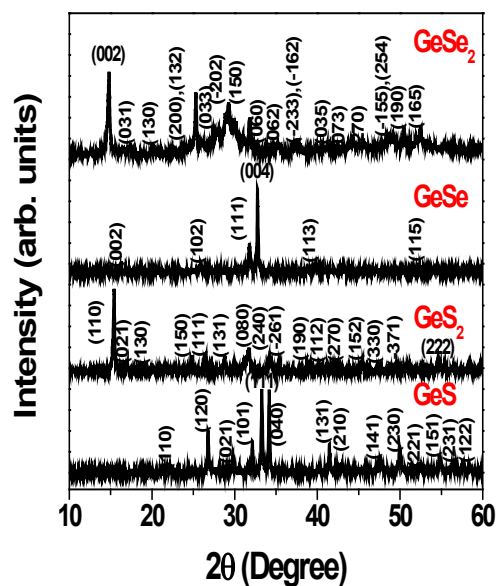


**Figure S4.** A plot of the S composition ( $x$ ) of  $\text{GeS}_x\text{Se}_{1-x}$  NC versus that of  $[\text{H}_2\text{S}]_x[\text{DMS}]_{1-x}$ , showing a linear correlation.

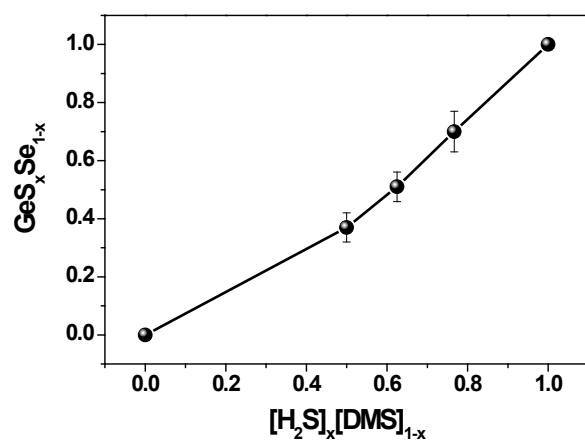


**Figure S5.** HRTEM image of GeS-CdS heterojunction NC, produced as an intermediate of cation exchange reaction, when the orthorhombic GeS NC was used instead of amorphous one. The CdS NC was grown on the side of GeS NC via cation substitution. Its corresponding FFT image of CdS NC is in the inset. The EDX data revealed the 2.8:1 ratio of Ge and Cd elements.

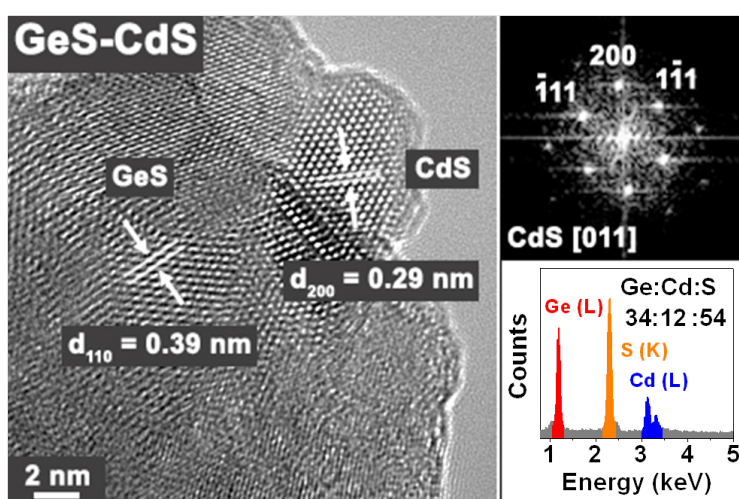


**Figure S6.** HRTEM images of (a) ZnS, (b) ZnSe, (c) CdS, (d) CdSe, (e) PbSe, (f) Ag<sub>2</sub>Se, (g) Ag<sub>2</sub>S, and (h) Ag-Ag<sub>2</sub>S. Its lattice resolved images insets. For ZnS, ZnSe, CdS, CdSe, and PbSe NC, the distances between the adjacent (111) planes were 3.1, 3.3, 3.4, 3.5, and 3.5 Å, respectively, which are close to those of the cubic phase. In the case of Ag<sub>2</sub>Se NC, the distance between the adjacent (200) planes was 2.5 Å, which are close to those of the cubic phase Ag<sub>2</sub>Se. The *d*-spacing of Ag<sub>2</sub>S NC was 3.1 Å, which are close to that of the orthorhombic phase Ag<sub>2</sub>S (111) planes. The Ag-Ag<sub>2</sub>S heterojunction NC was synthesized using 0.05 M AgNO<sub>3</sub>, in which the wire-like Ag<sub>2</sub>S NC forms a network between Ag NC. The *d*-spacing of Ag (111) planes and Ag<sub>2</sub>S (112) planes was identified as 2.4 and 2.5 Å, respectively. The average size of ZnS, ZnSe, CdS, and CdSe NC was estimated to be 4 nm. PbSe NC exhibits an average size of 10

nm. The size of  $\text{Ag}_2\text{Se}$  and  $\text{Ag}_2\text{S}$  NC is about 20 and 8 nm, respectively.

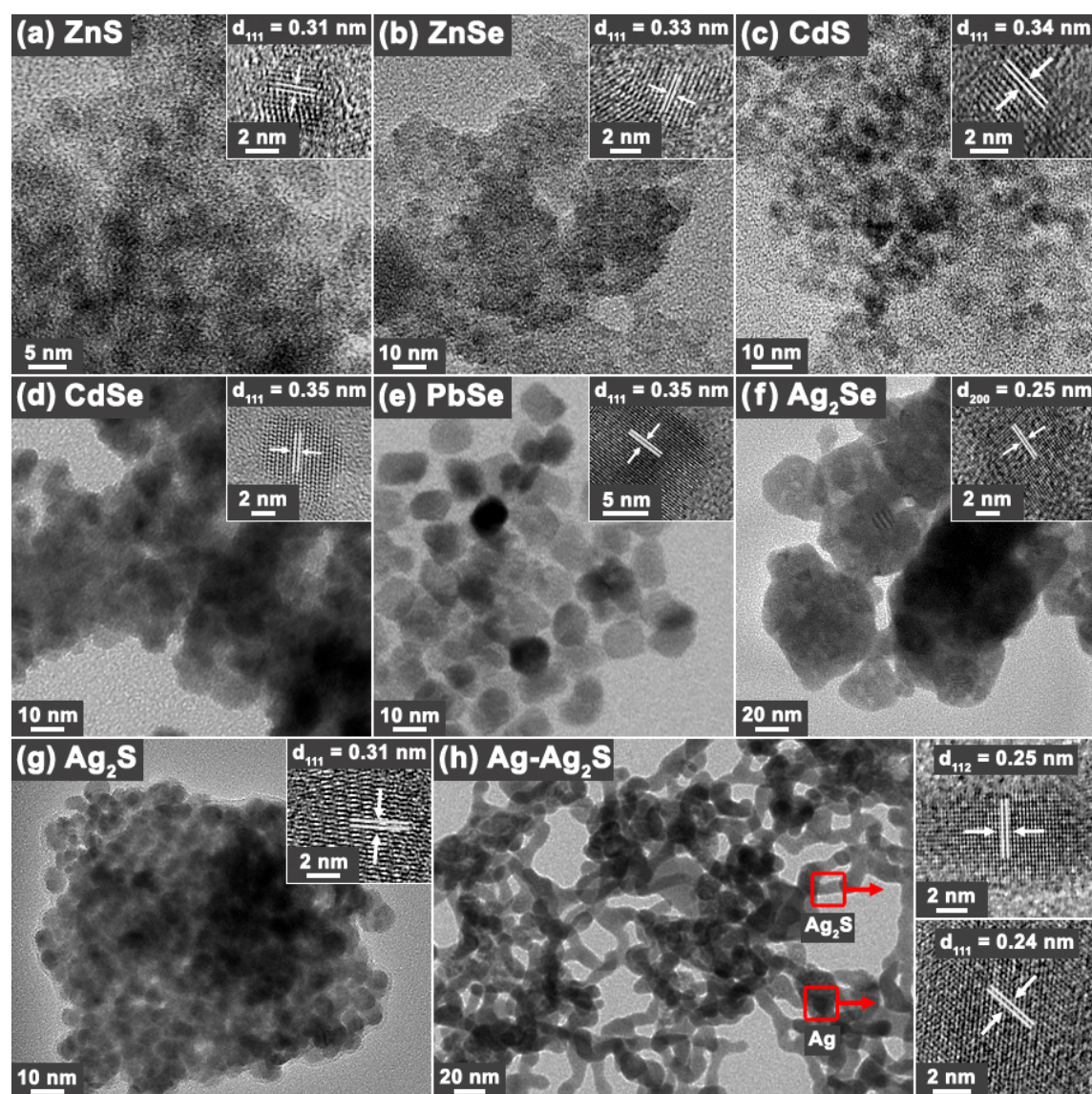


**Figure S7.** XRD pattern of  $\text{ZnS}$ ,  $\text{ZnSe}$ ,  $\text{Ag}_2\text{S}$ , and  $\text{Ag}_2\text{Se}$  NC. The peaks are indexed by the references; zinc blende  $\text{ZnS}$  (JCPDS No. 80-0020;  $a = 5.345 \text{ \AA}$ ), zinc blende  $\text{ZnSe}$  (JCPDS No. 80-0021;  $a = 5.618 \text{ \AA}$ ), monoclinic  $\text{Ag}_2\text{S}$  (JCPDS No. 14-0072;  $a = 4.229 \text{ \AA}$ ,  $b = 6.931 \text{ \AA}$ ,  $c = 7.862 \text{ \AA}$ ,  $\beta = 99.61^\circ$ ), cubic  $\text{Ag}_2\text{Se}$  (JCPDS No. 76-0135;  $a = 4.983 \text{ \AA}$ ) and orthorhombic  $\text{Ag}_2\text{Se}$  (JCPDS No. 71-2410;  $a = 4.333 \text{ \AA}$ ,  $b = 7.062 \text{ \AA}$ ,  $c = 7.764 \text{ \AA}$ ).

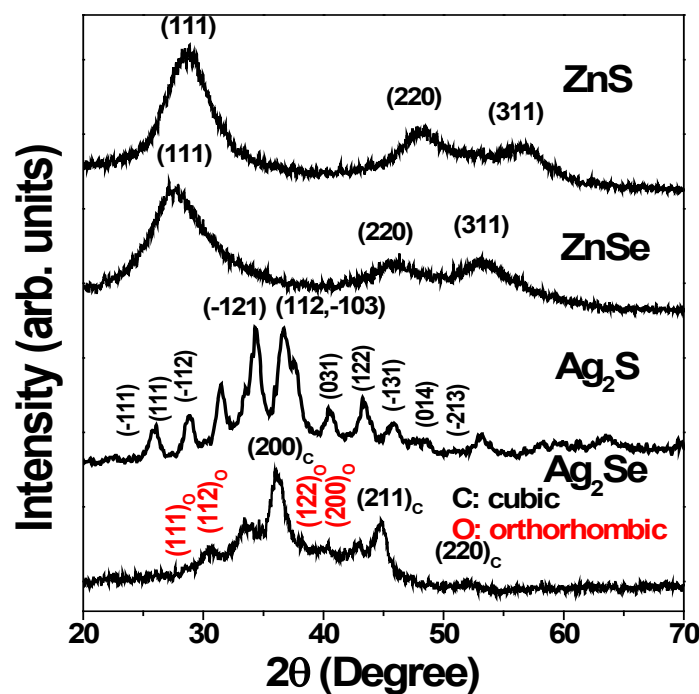


**Figure S8.** UV-visible spectrum of (a) amorphous and (b) orthorhombic GeS NC. The spectrum was used to estimate the band (indirect and direct) gaps by performing Kubelka-Munk transformations [A. Hagfeldt and M. Grätzel, *M. Chem. Rev.* **1995**, *95*, 49-68]. A plot of  $[ahv]^{1/2}$  and  $[ahv]^2$  (where  $\alpha$  is absorption coefficient) versus photon energy yielded indirect and direct band gap of 1.3 and 1.6 eV, respectively, for the amorphous GeS NC. The indirect and direct band gaps of orthorhombic phase GeS NC have been measured to be 1.6 eV. This result is consistent with the value of recent work on the orthorhombic GeS NC;  $E_g$  (indirect) = 1.58 eV,  $E_g$  (direct) = 1.61 eV) [Ref. 25: D. D. Vaughn, II; R. J. Patel, M. A. Hickner and R. E. Schaak, *J. Am. Chem. Soc.*, 2010, 132, 15170].

